Proc. Natl. Acad. Sci. USA
Vol. 88, pp. 6087–6091, July 1991
Biochemistry

Molecular structure of *Bacillus subtilis* aspartate transcarbamoylase at 3.0 Å resolution

(molecular replacement/pyrimidine biosynthesis/x-ray crystallography)

RAYMOND C. STEVENS, KARIN M. REINISCH, AND WILLIAM N. LIPSCOMB

Gibbs Chemical Laboratory, Harvard University, Cambridge, MA 02138

Contributed by William N. Lipscomb, March 25, 1991

ABSTRACT **The three-dimensional structure of *Bacillus subtilis* aspartate transcarbamoylase (ATCase; aspartate carbamoyltransferase; carbamoyl-phosphate:L-aspartate carbamoyltransferase, EC 2.1.3.2) has been solved by the molecular replacement method at 3.0 Å resolution and refined to a crystallographic *R* factor of 0.19. The enzyme crystallizes in the space group C2 with unit cell dimensions $a = 258.5$, $b = 153.2$, and $c = 51.9$ Å and $\beta = 97.7°$. The asymmetric unit is composed of three monomers related by noncrystallographic threefold symmetry. A total of 295 of 304 amino acid residues have been built into the monomer. The last 9 residues in the C terminus were not included in the final model. Each monomer consists of 34% α-helix and 18% β-strand. Three solvent-exposed loop regions (residues 69–84, 178–191, and 212–229) are not well defined in terms of electron density. The catalytic trimer of ATCase from *B. subtilis* shows great similarity to the catalytic trimer in *Escherichia coli* ATCase, which was used in constructing the model for molecular replacement. The unliganded trimer from *B. subtilis*, which is not cooperative, resembles the *T* (inactive) state slightly more than the *R* (active)-state form of the *E. coli* trimer. However, certain regions in the *B. subtilis* trimer exhibit shifts toward the *E. coli* R-state conformation.**

Aspartate transcarbamoylase (ATCase; aspartate carbamoyltransferase; carbamoyl-phosphate:L-aspartate carbamoyltransferase, EC 2.1.3.2) catalyzes the conversion of aspartate and carbamoyl phosphate to carbamoyl-L-aspartate in the first unique step of pyrimidine biosynthesis (1, 2). *Escherichia coli* ATCase has been studied extensively as a model for both homo- and heterotropic cooperativity (for reviews, see refs. 3–5). *E. coli* ATCase, representative of ATCase from enteric bacteria, consists of two catalytic trimers and three regulatory dimers, with a molecular weight of 320,000 (6, 7). The enzyme is cooperative with respect to carbamoyl phosphate and aspartate binding and is regulated by the nucleotides ATP, CTP, and UTP (8, 9). X-ray structures of the *E. coli* holoenzyme are known for both the *T* and *R* states with and without the nucleotide effectors (for reviews, see refs. 3–5).

The catalytic and regulatory subunits can easily be isolated after treating the holoenzyme with heat or mercurial compounds. The catalytic trimer, although catalytically active, no longer displays homotropic cooperativity (10). The isolated *E. coli* catalytic trimer can, however, be made cooperative by mutating arginine-105 to alanine (11). It was hoped that crystallographic studies of both the native and mutated *E. coli* trimers would elucidate further the mechanisms of cooperativity, and consequently attempts were made to grow crystals of the wild-type trimer suitable for structure determination. Thus far, however, these attempts have been unfruitful, and an alternative approach, the study of the catalytic trimer from *Bacillus subtilis*, which also lacks cooperativity, was pursued. Although it seems reasonable to expect that a mutation analogous to the Arg-105 → Ala mutation in *E. coli* could be made for *B. subtilis* ATCase, no site-directed mutagenesis experiment has been reported.

ATCase from *B. subtilis* is a catalytic trimer composed of 304 amino acids per monomer with an overall molecular weight of 102,000 (12, 13). The *B. subtilis* ATCase enzyme is interesting both because it will further elucidate the mechanism of homotropic cooperativity and because, belonging to a different class of ATCase enzyme from *E. coli*, the study will broaden the current view of the structure–function relationships in ATCase. Certainly, the structure of the *B. subtilis* enzyme will provide additional insight into hamster ATCase recently modeled by Scully and Evans (14). Hamster ATCase, though part of a three-enzyme complex, is also a catalytic trimer. In this respect it is more similar to *B. subtilis* than to *E. coli* ATCase, although the hamster and *E. coli* sequences share a greater sequence homology.

B. subtilis and *E. coli* ATCase share an overall sequence homology of 35% (43% for conservative residue replacement) as illustrated in Fig. 1 (15). All of the residues involved in binding the bisubstrate analogue *N*-(phosphonoacetyl)-L-aspartate (PALA) except for residue 267 in *E. coli* ATCase are conserved in the *B. subtilis* sequence. The homology is larger in the carbamoyl phosphate domain (43%) than in the aspartate domain (27%). This pattern, where the largest changes in sequence occur in the aspartate domain versus the carbamoyl phosphate domain, becomes apparent in the comparison between ATCase enzymes from any two sources (16). Consequently, we expected that changes in tertiary structure between *B. subtilis* and *E. coli* ATCase would be observed mainly in the aspartate domain and especially in connecting regions outside the core of the structure.*

MATERIALS AND METHODS

Protein Purification. The purification procedure used is a simplification of that proposed by Earl Ferguson in his bachelor's thesis (17) under the supervision of Robert Switzer at the University of Illinois. The protein was purified from the *E. coli* overproducing strain TB-2/pL2000 kindly provided to us by Robert Switzer. The bacteria were grown in 12-liter batches amid vigorous aeration in a fermentor. A solution of Na_2HPO_4 (6 g/liter), KH_2PO_4 (3 g/liter), NaCl (0.5 g/liter), NH_4Cl_2 (1 g/liter), Casamino acids (2 g/liter), and arginine (0.05 g/liter) was sterilized in the fermentor. To this solution we added $MgCl_2$ (1 ml of 1 M solution per liter), $CaCl_2$ (10 ml of 0.01 M solution per liter), and glycerol (5 ml), all autoclaved, and filter-sterilized ampicillin (50 mg/ml). Subse-

The publication costs of this article were defrayed in part by page charge payment. This article must therefore be hereby marked "*advertisement*" in accordance with 18 U.S.C. §1734 solely to indicate this fact.

Abbreviations: ATCase, aspartate transcarbamoylase; PALA, *N*-(phosphonoacetyl)-L-aspartate.

*The atomic coordinates have been deposited in the Protein Data Bank, Chemistry Department, Brookhaven National Laboratory, Upton, NY 11973 (reference 1AT2).

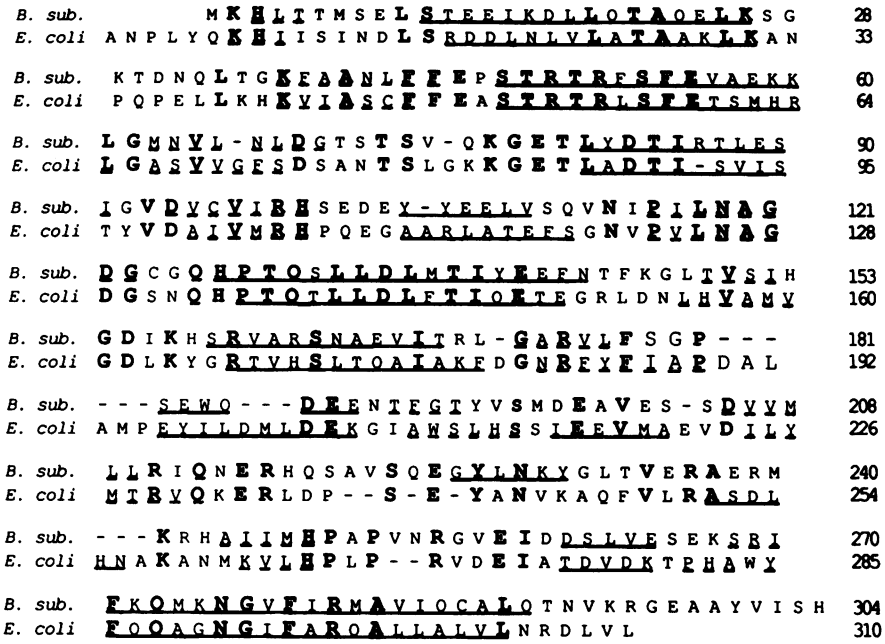

FIG. 1. The *B. subtilis* and *E. coli* sequences are aligned (15). Regions of α-helix are indicated with continuous lines and regions of β-strand are indicated by dashed lines. Boldface letters indicate sequence homology. Slight revisions of secondary structure are expected upon further refinement.

quently, 2 ml of an overnight culture was added to the nutrient broth. The bacteria were allowed to grow at 37°C until an optical density of 0.15 at 566 nm (≈6 hr) was attained. Filter sterilized β-D-thiogalactosidase (1 mM) was then added to the nutrient broth. After further growth, the bacteria reached the stationary phase at an optical density of 1.66 at 566 nm (≈8 hr more). The bacterial cells were concentrated by centrifugation for 20 min in a Beckman centrifuge, using a J-17 rotor at 8000 rpm. The supernatant was discarded, and the cells were resuspended in 0.5 liter of buffer A (50 mM Tris·HCl/10 mM $MgCl_2$/0.01 mM EDTA, pH 8.1). The cells were lysed with an Ultrasonics sonifier at the microtip limit and at 60% output setting. To prevent overheating, the cells were kept on ice during sonication and were sonicated in 30-sec pulses. Subsequent centrifugation with a J-14 rotor at 16,000 rpm for 20 min removed cell debris. The protein was precipitated by making the supernatant 80% saturated in $(NH_4)_2SO_4$ and was recovered by 15 min of centrifugation with a J-14 rotor at 15,000 rpm. The protein was redissolved in buffer B (50 mM Tris·HOAc/2 mM 2-mercaptoethanol, pH 8.3) and dialyzed against 2 × 8 liters of this buffer for a total of 18 hr. In the final step of purification, an ion-exchange column (Q Sepharose fast flow; Pharmacia) was used. The protein obtained from the previous step was separated into two batches, and each batch was run over 50 ml of column material. To elute ATCase, 0.75 liter of low-salt and 0.75 liter of high-salt buffer were used to make a gradient: the low-salt buffer was buffer B, the high-salt buffer was buffer B with 0.75 M NaCl. Fractions of 120 drops were collected and ATCase eluted after ≈100 fractions. Purity of the enzyme was determined by a SDS/polyacrylamide gel. For crystallization and storage purposes, the enzyme was dialyzed into a storage buffer (40 mM KH_2PO_4/1 mM 2-mercaptoethanol/1 mM NaN_3, pH 7.0) and concentrated to 12 mg/ml. The total yield of ATCase as measured by UV absorption at 280 nm was typically 600 mg per 12-liter batch as calculated by using an extinction coefficient of 0.57 cm^2/mg (13). Further purification by FPLC with a Pharmacia Mono Q column did not improve the quality of the crystals used in our present x-ray analysis, and the step was not included in the routine purification procedure.

Crystallization. Bar-shaped crystals (0.4 × 0.2 × 2.0 mm) were obtained by the hanging drop method. Drops consisting of a 1:1 (total drop volume, 30 μl) mixture of protein solution and buffer [1.7 M $(NH_4)_2SO_4$/0.1 M Tris·HCl, pH 8.5/2% PEG 200] were equilibrated against 1 ml of buffer at 21°C. Within a week crystals appeared, belonging to space group C2 with a = 258.5, b = 153.2, and c = 51.9 Å and β = 97.7°. The asymmetric unit contains one catalytic trimer. Solvent occupies ≈75% of the unit cell; the Matthews coefficient V_M (18) is 4.92. Although a 75% solvent content is high, it is not without precedent. For example, yeast phenylalanine tRNA crystallizes with a 71% solvent content (19), and influenza virus hemagglutinin crystallizes with a 78% solvent content (20).

Data Collection. Data to 3.0 Å resolution were collected at Boston College on a San Diego multiwire system area detector (21, 22) according to the data collection strategy of Xuong *et al.* (23). A total of 154,232 observations were recorded for 30,228 unique reflections. The reduced data are 83% complete between 10 and 3.0 Å with an R_{merge} value of 0.09 [$R_{merge} = \Sigma_{hkl}(\Sigma_i|I - \bar{I}|)/(\Sigma_i I)$].

Structure Determination. Five search models were used in the rotational and translational molecular replacement solutions (24): (*i*) a polyalanine trimer obtained by replacing the *R*-state (PALA liganded) *E. coli* catalytic trimer side chains (except for glycines) with methyl groups; (*ii*) a polyalanine trimer obtained by replacing the unliganded *T*-state *E. coli* catalytic trimer side chains (except for glycines) with methyl groups; (*iii*) an energy minimized model of the *B. subtilis* ATCase trimer built by molecular modeling of the *T*-state *E. coli* catalytic trimer; (*iv*) a polyalanine trimer version of the *B. subtilis* ATCase model; and (*v*) a monomer of the modeled polyalanine *B. subtilis*. The *B. subtilis* model was derived by building the *B. subtilis* sequence (15) into the structure of the *E. coli* catalytic trimer and subsequently minimizing the energy of the model by molecular dynamics; bond angles, bond lengths, and dihedral angles were idealized, and the van der Waals and electrostatic energies were minimized by using the X-PLOR 2.1 program (25).

Because the unit cell is flat with a c axis corresponding to the height of an *E. coli* catalytic trimer, the *B. subtilis*

catalytic trimer was expected to lie in the unit cell with a threefold axis roughly parallel to the *c* axis. A self-rotation function confirmed these expectations. Crowther's FFT program from the CCP4 package (26) as well as Brunger's X-PLOR 2.1 program (27, 28) were used for both the self-rotation and the rotation function. The threefold rotation axis lies 1° away from the *c* axis.

The CCP4 search was conducted in intervals of $\delta\alpha = \delta\beta = 2.5°$ and $\delta\gamma = 1.0°$, where angles have been defined according to the Daresbury convention, and the X-PLOR 2.1 search was conducted in intervals of 5° using Patterson correlation refinement for a more exact solution. Various resolution shells, including 5–8 Å, 5–9 Å, 5–10 Å, and 5–15 Å, were used in confirming the solution. The results from the two programs were identical. In both programs, the height of the peak corresponding to the solution was typically twice that of the next highest peak. All five molecular replacement models used produced similar results.

Both the CCP4 and X-PLOR 2.1 packages were used again in searching for the translational solution, but endeavors with CCP4 proved unsuccessful. X-PLOR 2.1 offered one clear solution more than 8 SD above the mean. This solution, reasonable in terms of crystal packing, was the one eventually used to generate phases. Various resolution shells, including 5–8 Å, 5–9 Å, 5–10 Å, and 5–15 Å, were used in confirming the solution. All five molecular replacement solutions produced similar results.

After the *B. subtilis* model was refined in one cycle of simulated annealing, the *R* factor dropped from 0.43 to 0.33 (25, 28). The initial maps showed clearly defined density in the carbamoyl phosphate domain but had several areas of discontinuous density in the aspartate domain. This preliminary result was similar to that obtained for the maps of *E. coli* ATCase at 3.0 Å resolution (29). At this stage we turned to model building using the molecular graphics package FRODO on an Evans and Sutherland picture system (30, 31). Five cycles of simulated annealing and model building brought the final *R* factor to 0.19. The averaged rms deviations are 0.028 Å and 4.6° for the bond lengths and angles, respectively. All refinements were completed using data $>4\sigma$ (28,662 reflections; 79% complete between 7 and 3 Å). The density in the final maps is good in both the carbamoyl phosphate and aspartate domains, although exceptions occur in solvent-exposed loops. Specifically, the electron density in residues 69–84, 178–191, and 212–229 is weak (Fig. 2). Residues 295–304 were not built into the structure due to a lack of electron density. A series of refined omit maps with 10 residues omitted at a time were consistent with the trace and sequence alignment; iterative noncrystallographic phase averaging confirmed the results.

RESULTS AND DISCUSSION

The catalytic monomers from *B. subtilis* ATCase, like those from *E. coli*, aggregate into trimers with C_3 symmetry in the approximate form of a disk with a radius and thickness of 50 Å (Fig. 3). As expected, the monomer consists of two domains, the carbamoyl phosphate and aspartate domains by analogy with ATCase from *E. coli*. The secondary structure includes 34% α-helix and 18% β-sheet. The carbamoyl phosphate domain contains four helices (residues 47–61, 83–89, 105–110, 128–142, and 271–290) partially surrounding a region of β-sheets (residues 2–6, 37–44, 63–69, and 94–101). A helix spanning residues 159–170 connects the carbamoyl phosphate domain, which has the larger α-helical content, to the aspartate domain. The aspartate domain has a core of parallel β-sheet (residues 149–152, 175–179, 205–210, 244–248, and 267–270) surrounded by several short α-helices (residues 182–188, 225–230, and 260–264). Weak density was seen for two of the last helices, probably because they are in solvent-exposed regions. Shown in Fig. 3 is the overall structure of the catalytic trimer of ATCase from *B. subtilis*. The average rms displacement (α-carbon atoms only) of the three catalytic chains in the asymmetric unit is 1.8 Å; the largest differences are found in the loop regions.

Not surprisingly, tertiary structures of the catalytic trimers from *B. subtilis* and *E. coli* exhibit great similarity. Fig. 4 shows the *B. subtilis* α-carbon backbone superimposed on the *T* (unliganded)- and *R* (PALA liganded)-state α-carbon backbones from the catalytic chain of the *E. coli* enzyme (32, 33). The rms difference between the α-carbon backbones of the *B. subtilis* and unliganded *T*-state *E. coli* catalytic chains is 1.1 Å. The rms difference between the *B. subtilis* and *E. coli* *R*-state catalytic chains is 1.2 Å. In both cases, the larger deviations of the *B. subtilis* structure from its *E. coli* model are in the region comprised of residues 60–90 and in the aspartate domain. With the exception of a short one-turn helix in *E. coli* (residues 215–220), which becomes a loop in

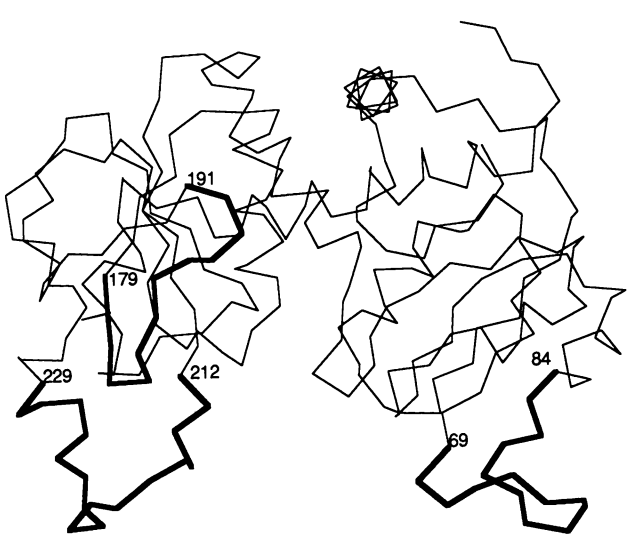

FIG. 2. A monomer is shown, with regions of weak and discontinuous density drawn with a thick line. These include residues 69–84, 179–191, and 212–229, all regions exposed to solvent.

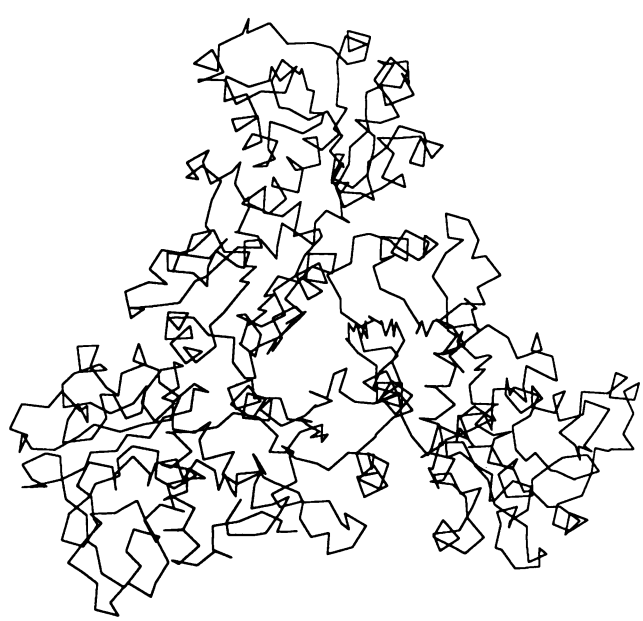

FIG. 3. Oligomeric state of *B. subtilis* ATCase looking down the noncrystallographic threefold axis.

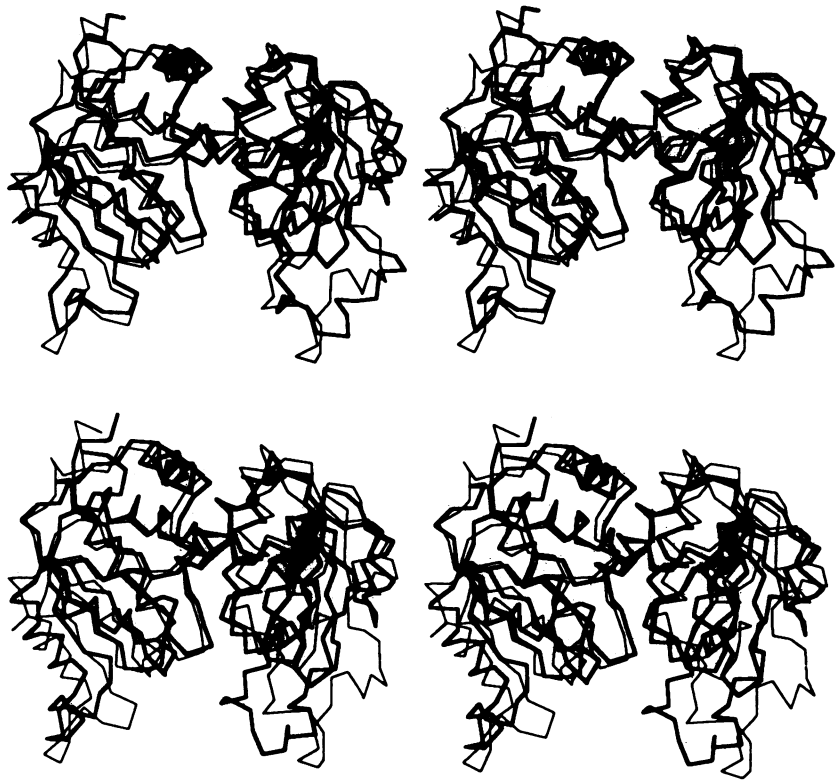

FIG. 4. (*Upper*) The catalytic monomer from *B. subtilis* ATCase (thin line) superimposed onto the *T*-state form of the catalytic monomer from *E. coli* (thick line). (*Lower*) The catalytic monomer from *B. subtilis* ATCase (thin line) superimposed onto the *R*-state form of the catalytic monomer from *E. coli* (thick line).

the *B. subtilis* structure, there are no changes in secondary structure.

The secondary structure predictions of Lerner and Switzer (15), based on the Chou–Fasman procedure, agree with the 3-Å structure in all but two regions. The helix predicted for residues 196–207 is absent from the structure, and the helix predicted for residues 234–244 spans residues 225–230. Previous biochemical studies have suggested the existence of a disulfide bond (12, 13). Such a bond is not observed in the crystal structure. The two closest cysteine sulfur atoms are located 10–13 Å apart depending on the catalytic chain under consideration.

Recently, Scully and Evans (14) have modeled the structure of hamster ATCase by using the coordinates of the *E. coli* PALA-ligated *R* state (33) as a starting point to investigate mammalian ATCase in its active form. Since the catalytic trimer is noncooperative, it is not known whether the inactive (*T*) or active (*R*) *E. coli* form more closely resembles the unliganded form of the *B. subtilis* enzyme. Until the liganded form of the *B. subtilis* trimer has been determined, caution should be exercised in discussing enzyme mechanisms.

The unliganded catalytic trimer of *B. subtilis* bears a slightly closer resemblance to the catalytic trimer of the *T*-state than the *R*-state ATCase from *E. coli*, where the carbamoyl phosphate and aspartate domains have moved closer together to form a narrower active site cleft than in the *T* state (Fig. 4). Nevertheless, the structure from *B. subtilis* does suggest small movements toward the *R*-state conformation. It is possible that ligation of carbamoyl phosphate to the enzyme will move the enzyme even closer to the *E. coli* *R*-state conformation. It is likely that the binding of PALA will induce the domain closure observed in the *R* state of ATCase from *E. coli*.

We thank R. Switzer and E. Ferguson at the University of Illinois for the overproducing strain of *B. subtilis* ATCase. We thank R. Kantrowitz and J. Stebbins at Boston College for the use of their laboratory, advice in growing large quantities of *B. subtilis* ATCase, and for permission to use their x-ray data collection facility. Hengming Ke is gratefully acknowledged for many useful discussions during the various stages of the project. We would like to thank James Wild for suggesting this experiment. We also thank the Pittsburg Supercomputing Center for the use of the Cray Y-MP, which allowed for rapid refinement of the crystal structure. This work was supported by National Institutes of Health Grant GM06920 (W.N.L.) and by National Institutes of Health postdoctoral fellowship (R.C.S.).

1. Jones, M. E., Spector, L. & Lipmann, F. (1955) *J. Am. Chem. Soc.* **77**, 819–820.
2. Reichard, P. & Hanshoff, G. (1956) *Acta Chem. Scand.* **10**, 548–566.
3. Kantrowitz, E. R. & Lipscomb, W. N. (1988) *Science* **241**, 669–674.
4. Kantrowitz, E. R. & Lipscomb, W. N. (1990) *Trends Biochem. Sci.* **15**, 53–59.
5. Stevens, R. C., Chook, Y., Cho, C. Y., Lipscomb, W. N. & Kantrowitz, E. R. (1991) *Protein Eng.* **4**, 391–408.
6. Weber, K. (1968) *Nature (London)* **218**, 1116–1119.
7. Wiley, D. C. & Lipscomb, W. N. (1968) *Nature (London)* **218**, 1119–1121.
8. Gerhart, J. C. & Schachman, H. K. (1965) *Biochemistry* **4**, 1054–1062.
9. Wild, J. R., Loughrey-Chen, S. J. & Corder, T. S. (1989) *Proc. Natl. Acad. Sci. USA* **86**, 46–50.
10. Hunt, J. B., Neeces, S. H., Schachman, H. K. & Ginsburg, A. (1984) *J. Biol. Chem.* **259**, 14793–14803.
11. Stebbins, J. W., Xu, W. & Kantrowitz, E. R. (1989) *Biochemistry* **28**, 2592–2600.
12. Brabson, J. S. & Switzer, K. L. (1975) *J. Biol. Chem.* **250**, 8664–8669.
13. Brabson, J. S., Maurizi, M. R. & Switzer, R. L. (1985) *Methods Enzymol.* **113**, 627–635.
14. Scully, J. L. & Evans, D. R. (1991) *Proteins* **9**, 191–206.
15. Lerner, C. G. & Switzer, R. L. (1986) *J. Biol. Chem.* **261**, 1156–1165.
16. Wild, J. R. & Wales, M. E. (1990) *Annu. Rev. Microbiol.* **44**, 93–118.

17. Ferguson, E. E., III (1990) Bachelor of Science Thesis (Univ. of Illinois, Urbana, IL).
18. Matthews, B. W. (1968) *J. Mol. Biol.* **33,** 491–497.
19. Kim, S. H., Quigley, G., Suddath, F. L., McPherson, A., Sneden, D., Kim, J. J., Weinzierl, J. & Rich, A. (1973) *J. Mol. Biol.* **75,** 429–432.
20. Wilson, I. A., Skehel, J. J. & Wiley, D. C. (1981) *Nature (London)* **289,** 366–373.
21. Hamlin, R. (1985) *Methods Enzymol.* **114,** 416–452.
22. Howard, A. J., Nielsen, C. & Xuong, N. H. (1985) *Methods Enzymol.* **114,** 452–472.
23. Xuong, N. H., Nielsen, C., Hamlin, R. & Anderson, D. (1985) *J. Appl. Crystallogr.* **181,** 342–350.
24. Rossmann, M. G. & Blow, D. M. (1962) *Acta Crystallogr.* **15,** 24–31.
25. Brünger, A. T. (1988) X-PLOR Manual (Yale University, New Haven, CT), Version 2.1.
26. Crowther, R. A. (1972) in *The Molecular Replacement Method,* ed. Rossman, M. G. (Gordon & Breach, New York), pp. 173–178.
27. Brünger, A. T. (1990) *Acta Crystallogr. A* **46,** 46–57.
28. Brünger, A. T., Krukowski, A. & Erickson, J. (1990) *Acta Crystallogr. A* **46,** 585–593.
29. Monaco, H. L., Crawford, J. L. & Lipscomb, W. N. (1978) *Proc. Natl. Acad. Sci. USA* **75,** 5276–5280.
30. Pfugrath, J., Saper, M. A. & Qiocho, F. A. (1984) in *Methods and Applications in Crystallographic Computing,* eds. Hall, S. & Ashiaka, T. (Clarendon Press, Oxford), pp. 404–407.
31. Jones, T. A. (1985) *Methods Enzymol.* **115,** 157–171.
32. Stevens, R. C., Gouaux, J. E. & Lipscomb, W. N. (1990) *Biochemistry* **29,** 7691–7702.
33. Krause, K. L., Volz, K. W. & Lipscomb, W. N. (1987) *J. Mol. Biol.* **193,** 527–553.